TECHNICAL MEMORANDUM

768

# Numerical sensitivity of the ECMWF model to Semi-Lagrangian departure point iterations

M. Diamantakis and L. Magnusson

Research Department

December 2015



European Centre for Medium-Range Weather Forecasts
Europäisches Zentrum für mittelfristige Wettervorhersage
Centre européen pour les prévisions météorologiques à moyen terme

Series: ECMWF Technical Memoranda

A full list of ECMWF Publications can be found on our web site under:
http://www.ecmwf.int/en/research/publications

Contact: library@ecmwf.int



European Centre for Medium-Range Weather Forecasts
Shinfield Park, Reading, RG2 9AX, England

**Abstract**

Computing the departure points (d.p.) is a fundamental calculation in a semi-Lagrangian numerical model. Most models compute these using a fixed point iteration scheme with a small number of iterations assuming that this is sufficient to converge. This assumption is tested here and results show that, for the long timesteps the ECMWF model IFS uses, convergence is not entirely satisfactory and improvement in forecast skill can be achieved by increasing the number of these iterations. There is a notable improvement in the vertical structure of tropical cyclones but also in the extra-tropical winds.

The impact of increasing the d.p. iterations in the IFS tangent linear (TL) model of the 4DVAR data assimilation system is also tested. Surprisingly, increasing the iterations in the TL model occasionally excites an instability in the stratosphere in regions of strong jets. This seems to happen when iterations do not converge to a fixed point. An algorithm is proposed here in which stopping criteria based on convergence rate are used to terminate iterations when such a non-converging situation is anticipated. Testing shows that this is sufficient to prohibit development of this instability and it is possible to run the 4DVAR system with increased number of d.p. iterations consistently with the nonlinear forecast model.

# 1 Introduction

The ECMWF forecast model IFS employs a semi-Lagrangian semi-implicit discretization in time in combination with a spectral transform technique for solving the prognostic equations of the atmosphere (ECMWF, 2015). The semi-Lagrangian (SL) method is applied on the advection terms of the equations while semi-implicit time discretization is applied on the remaining terms. Here we are focusing on the SL advection scheme and in particular on the convergence properties of the technique employed to compute the departure points of SL trajectories.

Consider the following general form of the prognostic equations:

$$\frac{DX}{Dt} = F_X, \quad \frac{D}{Dt} = \frac{\partial}{\partial t} + \mathbf{V}\cdot\nabla, \qquad \mathbf{V} = (u, v, \dot{\eta}) \tag{1}$$

$$\frac{D\mathbf{r}}{Dt} = \mathbf{V}(\mathbf{r}, t) \tag{2}$$

where $X$ a prognostic variable, $F_X$ represents the forcing terms, $\mathbf{r}$ denotes the position of an air parcel which moves with velocity $\mathbf{V}$. The two time-level, semi-Lagrangian, semi-implicit discretization of (1) used in IFS (see Temperton et al., 2001) may be written:

$$\frac{X_A^{t+\Delta t} - X_D^t}{\Delta t} = \frac{1}{2}\left(L_D^t + L_A^{t+\Delta t}\right) + \frac{1}{2}\left(N_D^{t+\Delta t/2} + N_A^{t+\Delta t/2}\right)$$

where the forcing term $F$ has been split in a fast changing linear term $L$ and a slow changing nonlinear term $N$ using an appropriate reference state (for details see Temperton et al., 2001). The unknown term $N^{t+\Delta t/2}$ can be obtained by extrapolation. The subscript A denotes values at the arrival points (gridpoint values) and subscript $D$ denotes field values interpolated at the departure points (d.p.) of the Lagrangian trajectory of a fluid parcel. The assumption is that a parcel starts its trajectory at time $t$ at the departure point and terminates at $t+\Delta t$ on the arrival point. The d.p. is unknown and is computed integrating (2)

in $[t, t+\Delta t]$ and discretizing the integral. Using the mid-point rule technique we obtain:

$$\mathbf{r} - \mathbf{r_D} = \Delta t \mathbf{V}_M^{t+\Delta t/2}, \quad \mathbf{V}_M^{t+\Delta t/2} \approx \mathbf{V}\left(\frac{\mathbf{r}+\mathbf{r_D}}{2}, t+\frac{\Delta t}{2}\right) \tag{3}$$

Eq. (3) can be solved for $\mathbf{r_D}$ iteratively interpolating the wind field at the trajectory midpoint at each new iteration. As the wind field is needed at $t+\Delta t/2$ time extrapolation is utilised. The method used in IFS is based on SETTLS scheme (Stable Extrapolation Two Time-Level Scheme by Hortal, 2002, recently revised with a vertical limiter to resolve noise issues in the upper stratosphere, see Diamantakis, 2014):

$$\mathbf{r}_D = \mathbf{r} - \frac{\Delta t}{2}\left\{\mathbf{V}^t + \left[2\mathbf{V}^t - \mathbf{V}^{t-\Delta t}\right]_D\right\} \tag{4}$$

where the wind field values at $D$ are obtained by interpolation. The scheme defines an implicit equation which is solved iteratively:

1. Store: $\mathbf{V}^{ext} = 2\mathbf{V}^t - \mathbf{V}^{t-\Delta t}$
2. Initialise: $\mathbf{r_D}^{(1)} = \mathbf{r} - \Delta t \mathbf{V}^t(\mathbf{r})$
3. For $\ell = 2, 3, \ldots$:
   (a) Interpolate $\mathbf{V}^{ext}$ to latest computed d.p. $\mathbf{r_D}^{(\ell-1)}$ : $\mathbf{V}^{ext}\left(\mathbf{r_D}^{(\ell-1)}\right)$
   (b) Apply SETTLS: $\mathbf{r}_D^{(\ell)} = \mathbf{r} - 0.5\Delta t\left[\mathbf{V}^t + \mathbf{V}^{ext}\left(\mathbf{r_D}^{(\ell-1)}\right)\right]$

The above sequence means that after an initial estimation of the d.p. using an explicit Euler formula, further iterations are done using SETTLS. Here for simplicity, without loss of generality we have shown how the iterative scheme is applied in a simple Cartesian coordinate system. In the actual IFS model the mathematical details are more complex as spherical geometry has to be taken into account for the horizontal part.

Different models use different extrapolation methods but all with a a small number of iterations, typically 2 or 3, to solve the derived implicit equation (3). This choice was the outcome of investigations made decades ago using early SL models which did not demonstrate any benefit by using large number of iterations, for example see Staniforth and Côté (1991). In Section 2 of this report we will challenge this assumption in the context of IFS by investigating the convergence of the departure point iterative scheme and looking at its performance during extreme conditions regarding wind speeds. In Section 3 we present results from forecast experiments which demonstrate that increasing the number of d.p. iterations improves the forecast accuracy particularly when long timesteps are used. In Section 4 we discuss the implementation of an algorithm that allows IFS to determine the most appropriate number of d.p. iterations for each gridpoint based on convergence rate criteria, as repeating non-converging iterations can occasionally lead to an instability in the tangent linear forecast model used by the IFS 4DVAR data assimilation system in the stratosphere. The algorithm discussed here ensures that the model remains stable when such situation occurs.

## 2 Diagnostics of convergence with respect to departure point iterations (DPI)

In operational configurations of IFS, d.p. iterations, henceforth DPI, stop at $\ell = 3$ assuming that convergence to sufficient accuracy has been achieved. To test whether this setting is sufficient for convergence

we have increased the number of DPI in IFS from the default value 3 to 5 and plotted the scaled difference of two successive estimates of the d.p., at iterations $\ell-1$, $\ell$, for the horizontal and the vertical part i.e.

$$\delta x_{D,ik}^{(\ell)} = \frac{\left| x_{D,ik}^{(\ell)} - x_{D,ik}^{(\ell-1)} \right|}{d_k}, \quad \ell = 2,3,\ldots \tag{5}$$

where $ik$ denotes the $i^{th}$-gridpoint of the $k^{th}$ level. For the vertical $x_D = \eta_D$ i.e. $x_D$ is the vertical coordinate of the d.p. while $d_{ik}$ is the thickness of the layer defined by two adjacent vertical model levels $k-1$, $k$. For the horizontal, $x_{D,ik}$ is taken to be the horizontal distance (geodesic length) of the d.p. from the arrival (grid) point. It is approximately equal to $\alpha\phi_{D,ik}^{(\ell)}$ where $\alpha$ is the distance of gridpoint $ik$ from the centre of the earth, $\phi_{D,ik}^{(\ell)}$ is the angle formed between gridpoint $ik$, the centre of the earth and the $\ell^{th}$ iteration estimate of the d.p. for this gridpoint. Here, $d_{ik}$ is constant and is set equal to the horizontal grid resolution e.g. for TL1279 spectral resolution (on a linear Gaussian grid) will be approximately 16km.

In Fig. 1 the convergence diagnostic (5) is plotted for $\ell = 2,3,4,5$ at t+48 hrs for a forecast starting at 10 January 2014 and for IFS level 96 (approximately 500hPa). The horizontal resolution is TL1279 while 137 levels have been used in the vertical. It is clear that 3 iterations are not enough for the d.p. calculation to converge as $\delta x_D^{(4)}$, $\delta x_D^{(5)}$ are relatively large, especially in the vertical direction, over the Himalaya, the Rockies and the Andes. Therefore, for some gridpoints in these regions and this model level the extra 4th iteration may significantly adjust the estimate of the departure point obtained by the 3rd iteration. This correction might look small but is comparable with the magnitude of the thickness $d_{ik}$. Considering that this difference may accumulate over many timesteps it is likely that it will have a systematic impact in forecast accuracy. The 5th iteration further adjusts the d.p. but as this is much smaller we could safely assume that no further iterations are needed. This assumption is re-enforced by verification tests which show that using more than 5 iterations does not improve further the quality of the forecast. Similar conclusions can be reached from analysing a summer case such as the one shown in Fig. 2, where the diagnostic (5) is plotted again at model level 96 (approximately 500hPa) and at t+48 hrs. For $\ell = 4,5$ the largest corrections to the d.p. are computed in the Andes and Antarctic region where the flow is strongest. A very localised correction is located between the Philippines and Japan. This correction coincides with the tropical cyclone Neoguri and will be investigated in the next section. Repeating the same forecasts but with half the timestep $\Delta t$=600s used at TL1279 resolution we notice that the increments added to departure points beyond the 3rd iteration are much smaller and therefore, with $\Delta t$=300s, there is no significant benefit by increasing the number of DPI.

Overall, the sufficient condition for convergence of DPI (see Pudykiewicz and Staniforth, 1984; Smolarkiewicz and Pudykiewicz, 1992) that the Lipschitz number must be less than 1 is satisfied. Typically, values are smaller than 0.1. However, we have found that in extreme cases, with the long timesteps used in the IFS, it is possible for the Lipschitz number to approach or even slightly exceed 1 for a very small number of gridpoints. Such cases are strong stratospheric polar jets and deep tropical cyclones where the horizontal and vertical wind shear is very large.

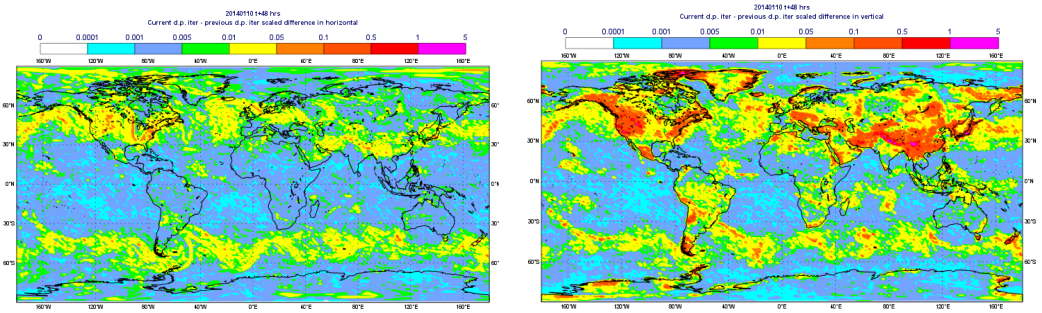

(a) horizontal $\delta x^{(2)}_{D,ik}$ (b) vertical $\delta x^{(2)}_{D,ik}$

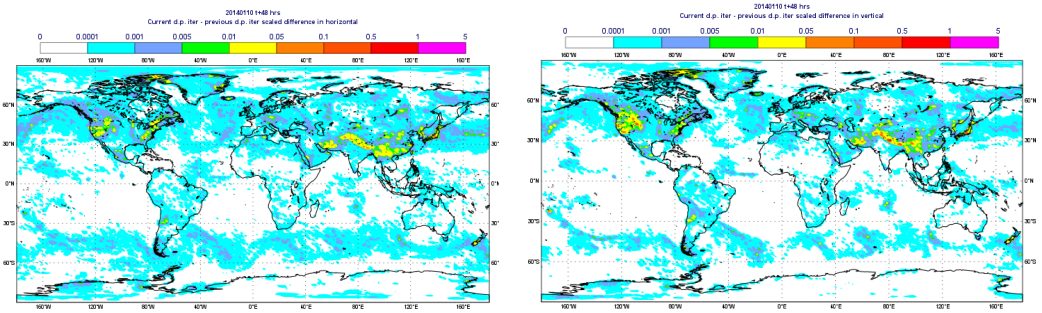

(c) horizontal $\delta x^{(3)}_{D,ik}$ (d) vertical $\delta x^{(3)}_{D,ik}$

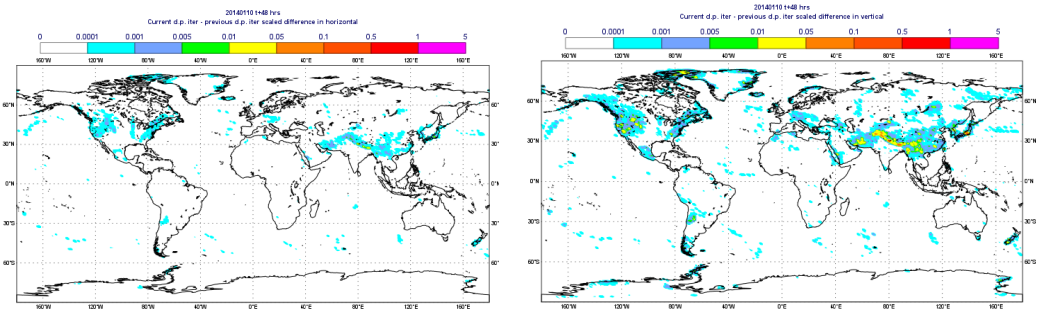

(e) horizontal $\delta x^{(4)}_{D,ik}$ (f) vertical $\delta x^{(4)}_{D,ik}$

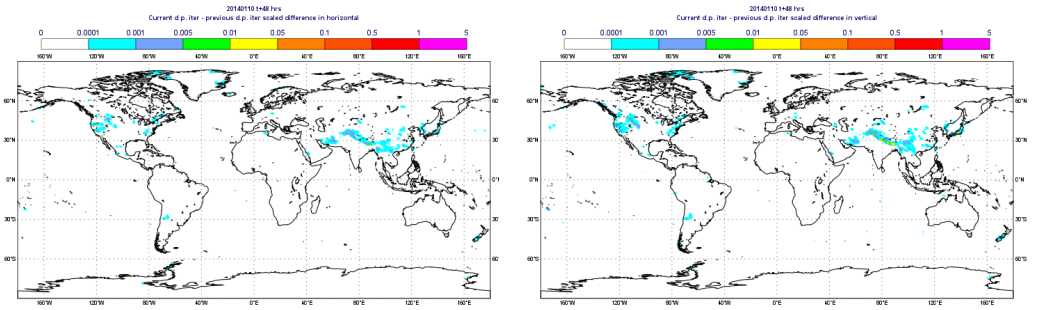

(g) horizontal $\delta x^{(5)}_{D,ik}$ (h) vertical $\delta x^{(5)}_{D,ik}$

Figure 1: Horizontal (a,c,e,g) and vertical (b,d,f,h) scaled d.p. iteration difference $\delta x^{(\ell)}_{D,ik}$, $\ell = 2,3,4,5$ at level 96, 10 January 2014, t+48 hrs.

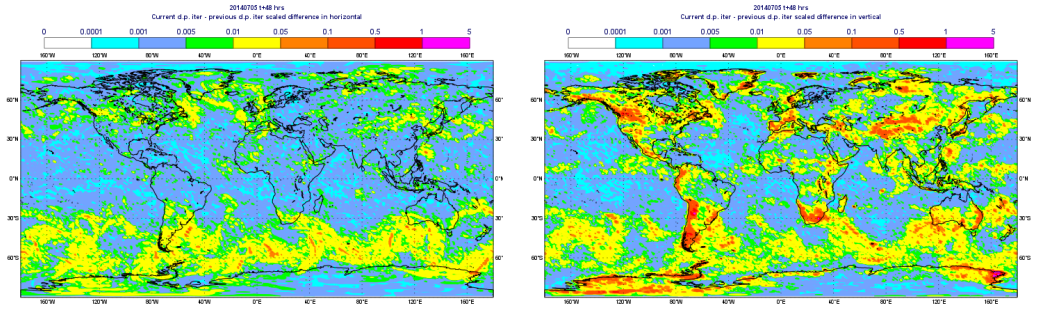

(a) horizontal $\delta x_{D,ik}^{(2)}$ (b) vertical $\delta x_{D,ik}^{(2)}$

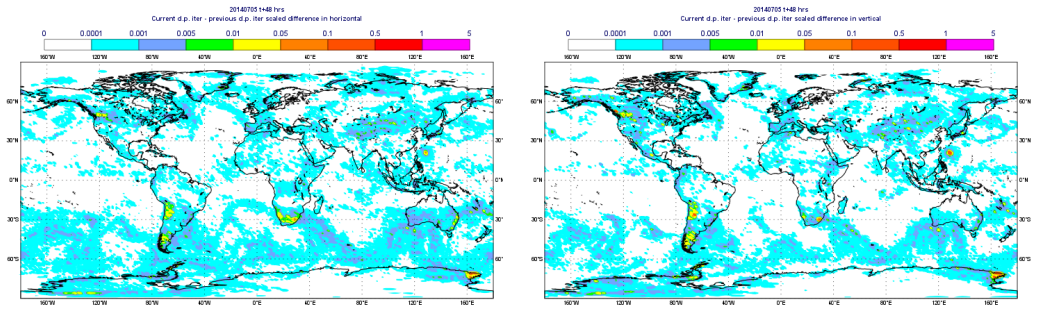

(c) horizontal $\delta x_{D,ik}^{(3)}$ (d) vertical $\delta x_{D,ik}^{(3)}$

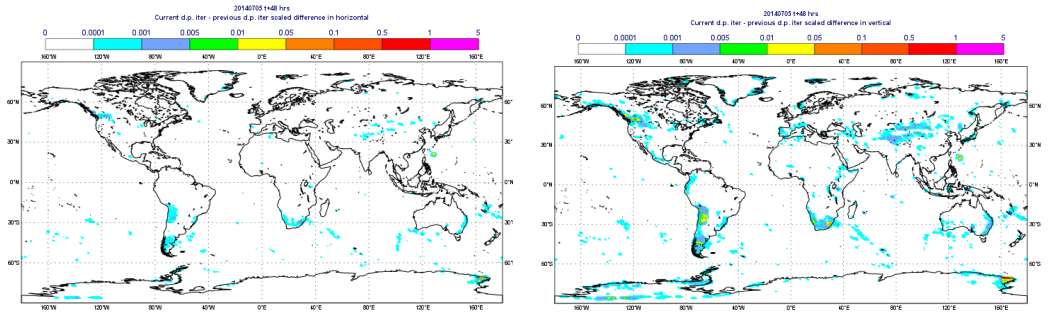

(e) horizontal $\delta x_{D,ik}^{(4)}$ (f) vertical $\delta x_{D,ik}^{(4)}$

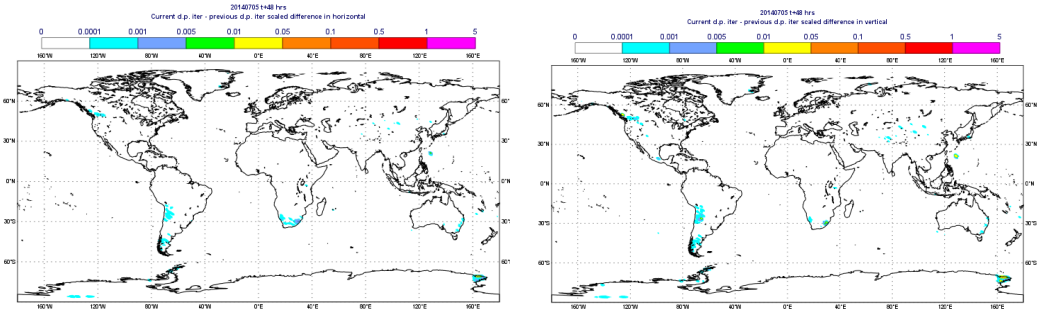

(g) horizontal $\delta x_{D,ik}^{(5)}$ (h) vertical $\delta x_{D,ik}^{(5)}$

Figure 2: Horizontal (a,c,e,g) and vertical (b,d,f,h) scaled d.p. iteration difference $\delta x_{D,ik}^{(\ell)}$, $\ell = 2,3,4,5$ at level 96, 5 July 2014, t+48 hrs.

## 2.1 Impact on tropical cyclones

The test case of tropical cyclone (TC) Neoguri is used here to demonstrate the impact of d.p. iterations for a specific atmospheric feature. Tropical cyclones are a stern test for an advection scheme as both the horizontal and vertical velocities are extreme. Four experiments are presented here: (a) a control forecast at TL1279 resolution using the default timestep $\Delta t = 600$s and 3 iterations (b) the same forecast but with 5 iterations (c) $\Delta t = 300$s and 5 iterations and (d) $\Delta t = 200$s and 5 iterations. TC Neoguri reached maximum intensity of 930 hPa on 7 July 2014 and later made landfall on southern Japan. It is worth noticing here that the operational ECMWF predicted a too strong intensity and the forecast from 5 July 00UTC predicted a minimum pressure of below 900 hPa.

A vertical east-west cross-section of the potential vorticity field crossing the typhoon core is shown in Fig. 3a-d at t+96 hrs. At this step very noticeable differences have developed in the simulation. As the exact typhoon track is sensitive to small perturbations (such as the ones introduced by the model changes here) the east-west cross sections passing from the centre of the core had to be taken at slightly different latitudes. These simulations show striking differences particularly in the stratosphere where in case (a) appears very noisy with pockets of negative PV reaching up in the stratosphere. Increasing the number of DPI to 5 removes this noise and gives a forecast which is closer to the short timestep forecasts (c) and (d). Even these differ noticeably which shows the sensitivity of the simulation. However, none is noisy in the stratosphere including forecast (b) where the standard long timestep is used which demonstrates the improvement obtained by increasing iterations.

The instabilities caused by the negative PV create significant vertical velocities and increased mixing into the stratosphere. Fig. 3e-h shows the specific humidity at 50 hPa for the same forecasts and time step as in Fig. 3a-d (units g/kg). The simulation with 3 iterations has as maximum of 41 g/kg in the vicinity of Neoguri, while no other place on the globe for this step exceeded 3 g/kg (not shown). In the simulations with 5 iterations the specific humidity on this level maintains a very small value throughout the forecast and the same hold true for the simulations with shorter time step.

Ploting the d.p. iteration diagnostic $\delta x_D^{(1)}$,...,$\delta x_D^{(4)}$ as before reveals an interesting pattern as illustrated in Fig. 4. The convergence seems to be slow in the region of the typhoon both in the horizontal and the vertical and certainly by the end of iteration 3, it has not converged. The two extra DPI are correcting significantly the d.p. estimates. In this case even more than 5 iterations are needed for the DPI to converge, however, the extra benefit obtained by going beyond the $5^{th}$ iteration is small. Using a shorter timestep $\Delta t/2$ improves the convergence as we can see in Fig. 5.

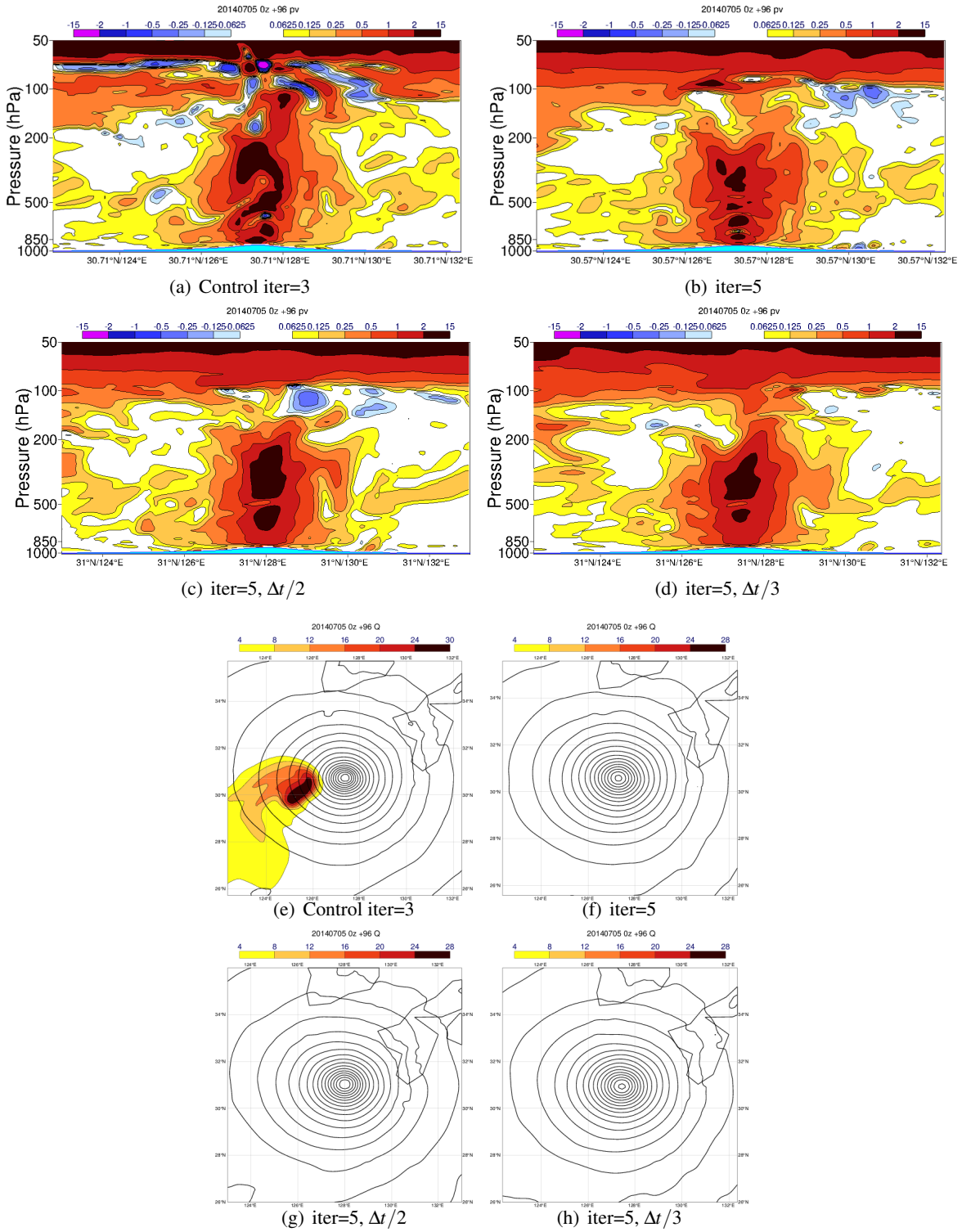


(a) Control iter=3 (b) iter=5

(c) iter=5, $\Delta t/2$ (d) iter=5, $\Delta t/3$

(e) Control iter=3 (f) iter=5

(g) iter=5, $\Delta t/2$ (h) iter=5, $\Delta t/3$

Figure 3: (a)-(d): East-west vertical cross section of potential vorticity field for three simulations of hurricane Neoguri. (e)-(h):t+96hrs specific humidity (g/kg) at 50hPa above the core of Neoguri.

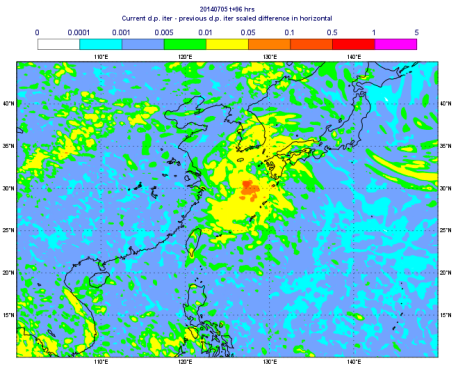

(a) horizontal $\delta x^{(2)}_{D,ik}$

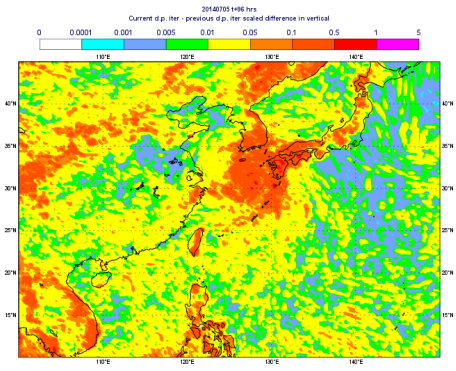

(b) vertical $\delta x^{(2)}_{D,ik}$

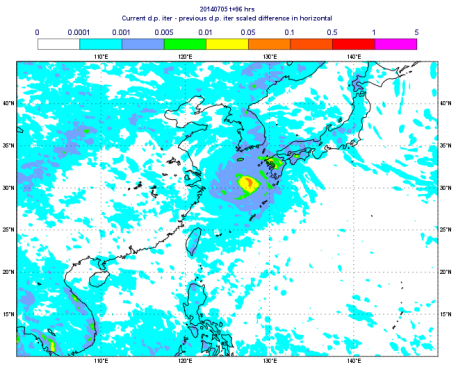

(c) horizontal $\delta x^{(3)}_{D,ik}$

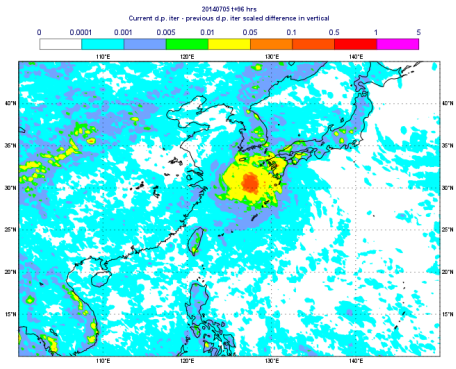

(d) vertical $\delta x^{(3)}_{D,ik}$

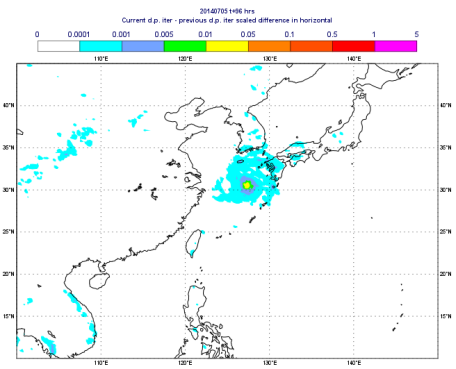

(e) horizontal $\delta x^{(4)}_{D,ik}$

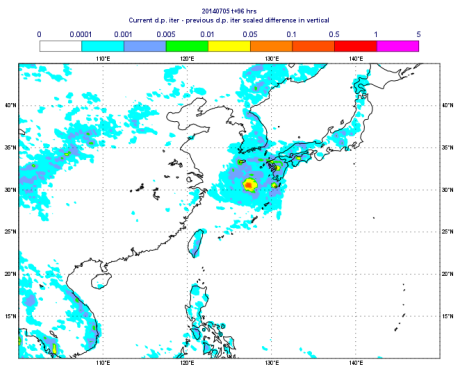

(f) vertical $\delta x^{(4)}_{D,ik}$

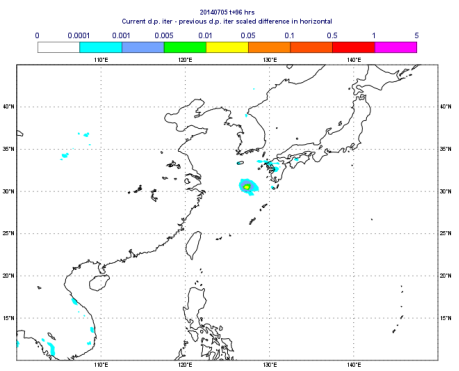

(g) horizontal $\delta x^{(5)}_{D,ik}$

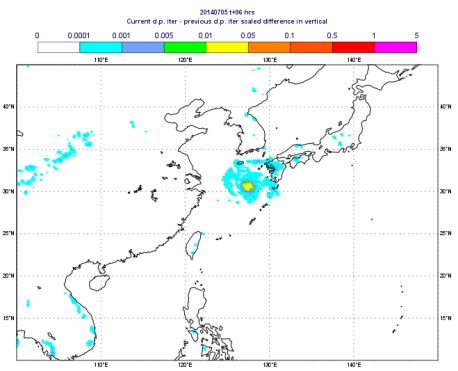

(h) vertical $\delta x^{(5)}_{D,ik}$

Figure 4: Horizontal (a,c,e,g) and vertical (b,d,f,h) scaled d.p. iteration difference $\delta x^{(\ell)}_{D,ik}$, $\ell = 2,3,4,5$ at t+96 hrs 850 hPa in the region of typhoon Neoguri.

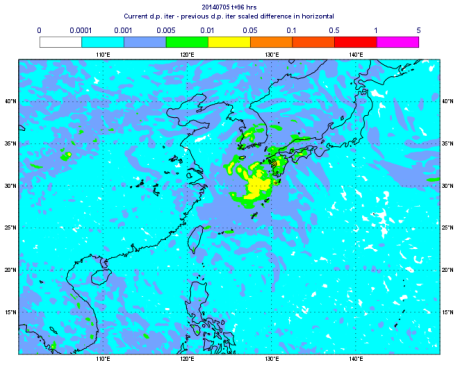

(a) horizontal $\delta x^{(2)}_{D,ik}$

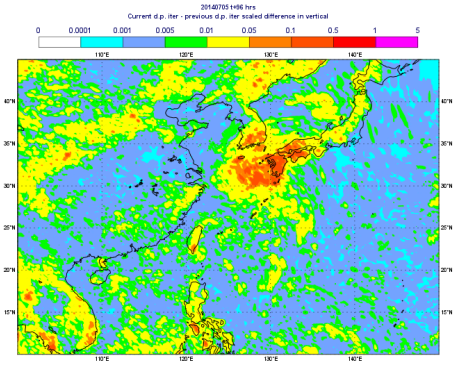

(b) vertical $\delta x^{(2)}_{D,ik}$

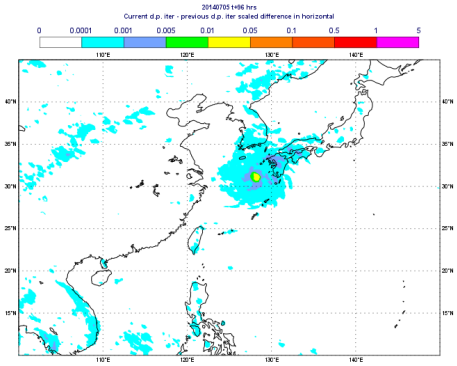

(c) horizontal $\delta x^{(3)}_{D,ik}$

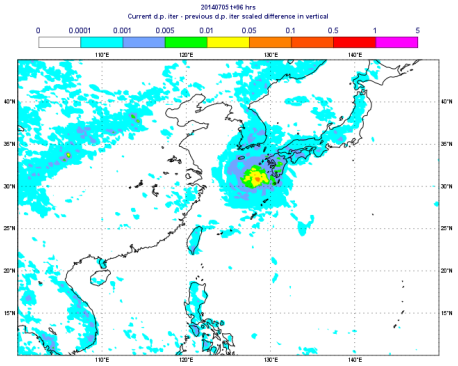

(d) vertical $\delta x^{(3)}_{D,ik}$

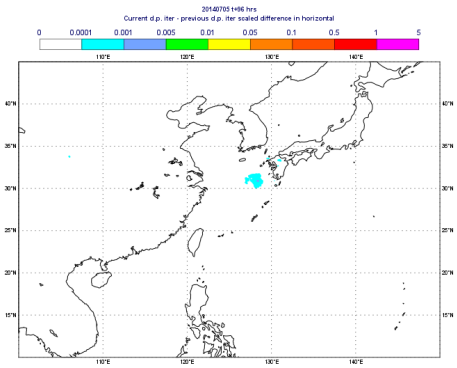

(e) horizontal $\delta x^{(4)}_{D,ik}$

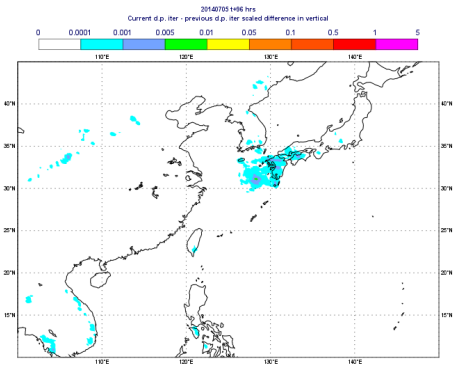

(f) vertical $\delta x^{(4)}_{D,ik}$

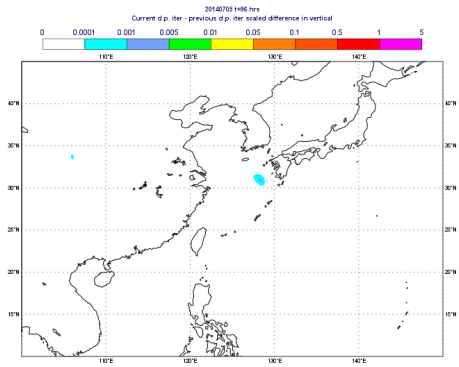

(g) vertical $\delta x^{(5)}_{D,ik}$

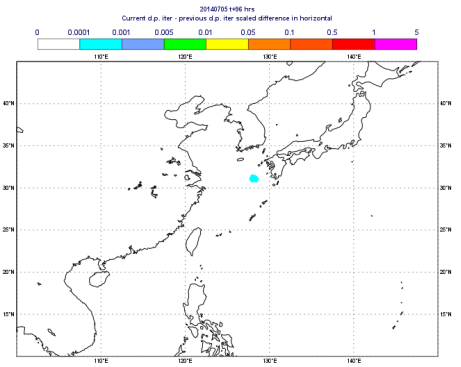

(h) horizontal $\delta x^{(5)}_{D,ik}$

Figure 5: Horizontal (a,c,e,g) and vertical (b,d,f,h) scaled d.p. iteration difference $\delta x^{(\ell)}_{D,ik}$, $\ell = 2,3,4,5$ at t+96 hrs 850 hPa in the region of typhoon Neoguri from forecast with $\Delta t/2$.

# 3 Verification results

To demonstrate the impact on forecast quality, an experiment using 5 DPI for the period 1/01/2014 to 15/02/2014 at high resolution (Tco1279 using an octahedral cubic grid, approximately 9km spacing, see Wedi et al., 2015) is compared with a similar experiment using the standard setting of 3 DPI. Both experiments use the same initial conditions i.e. forecasts have been started by the same analysis and the forecasts have been verified against this analysis.

Fig. 6a shows the root-mean-square (RMSE) difference for the geopotential height at 500 hPa for 4-day forecasts. A large reduction of RMSE is noticeable in a region at the east of the Himalayas. For a summer experiment (not shown), a similar reduction is present in the east of the Andes. The reduction in RMSE is mainly connected to a reduced bias. The improvement is not only confined to the geopotential height but we also find it in the tropospheric temperatures and the winds on the jetstream level (in the same region). The reduced RMSE is just downstream of the region where iteration 4, 5 increments to the d.p. are largest. (Fig. 1). The precipitation bias over China is also reduced in the experiment with 5 iterations (not shown). Whether this reduction is an indirect effect of the improved flow or a direct effect by a reduction in vertical instabilities in the model is not fully understood yet.

The RMSE for humidity at 50hPa is plotted in Fig. 6b. There is a noticeable reduction of RMSE for the relative humidity field (and temperature) on this level in the stratosphere over the south Pacific. This is linked with improved tropical cyclone performance as discussed in the previous section and shows that it also impacts the averaged scores over 1.5 months (the main tropical cyclone activity in January can be found in the south-western Pacific). As tropical cyclones are rare and the effect is, although large in amplitude, limited in time, the results are in general not statistically significant. But as we understand the process behind the improvement we recognise the result as important.

An additional experiment was undertaken with a longer model timestep (450s). Compared to the experiment with 3 DPI and 400s timestep, similar improvements were found as with 400s timestep (not shown). This demonstrates that by increasing the number of DPI from 3 to 5 the model can use a longer timestep, saving CPU time and still improve the accuracy of the forecast. The improvements do not occur when keeping the DPI to 3 and increasing the timestep, on the contrary a small deterioration is observed. It is worth mentioning that the CPU overhead by raising the DPI from 3 to 5 is very small, close to 1% while the savings achieved by increasing $\Delta t$ is 12.5%. As a result, 450s timestep and 5 DPI has been chosen for the new high resolution system (Tco1279) which is expected to be implemented operationally in 2016.

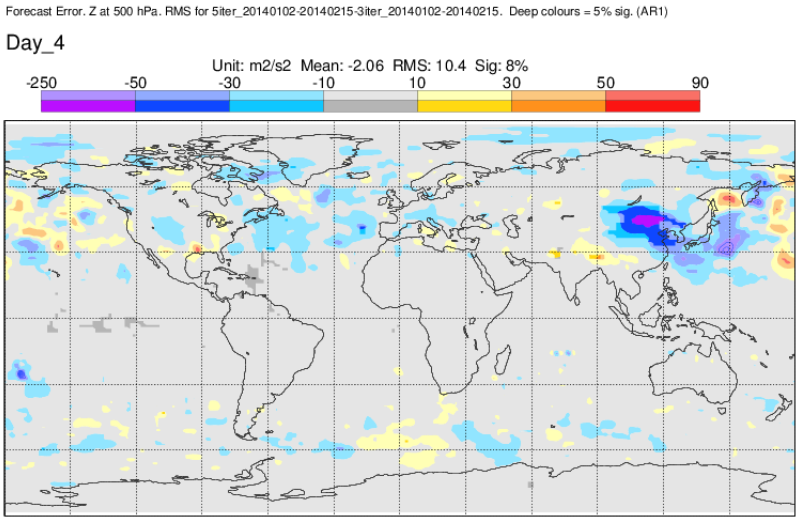


(a) z 500 hPa RMSE difference

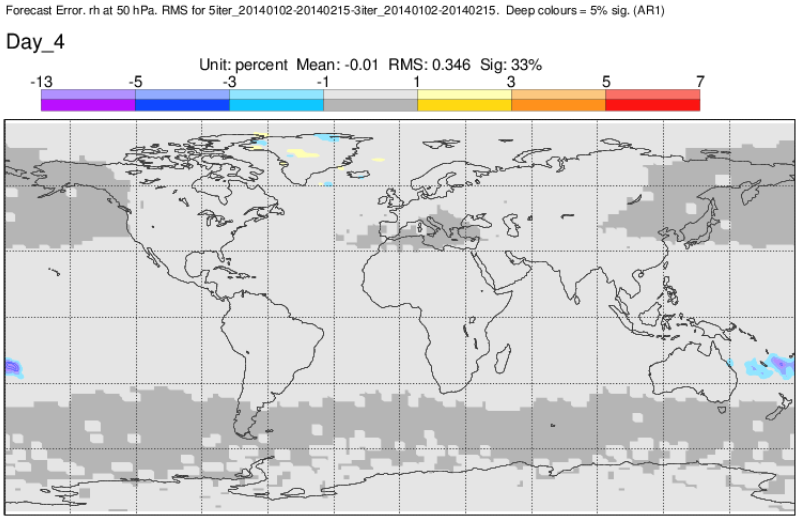


(b) RH 50 hPa RMSE difference

Figure 6: Top: RMSE differences between forecast with 3 DPI, $\Delta t = 400s$ and forecast with 5 DPI, $\Delta t = 400s$ both at t+96 hrs. Blue colours indicate reduction of RMSE. Bold colours indicate statistically significant results at 95% level. Bottom: same RMSE difference for relative humidity field at 50 hPa.

# 4 Convergence control and dynamic selection of DPI

The results in the previous sections indicate that d.p. at different areas on the globe converge at different rates and a small percentage may not converge at all. This is either because the convergence rate is too slow or because of divergent DPI i.e. the distance of d.p. estimates grows instead of shrinking with increased number of iterations. This occurs in cases of extreme winds and very high wind shear associated with large Lipschitz numbers. Hence, it may be beneficial to have a control mechanism in the model to stop DPI once there is an indication that they begin to diverge or when they have converged.

To implement such strategy we shall first define the *ik* gridpoint convergence rate to be:

$$cr_{ik} = \frac{\| x_{D_{ik}^{(\ell)}} - x_{D_{ik}^{(\ell-1)}} \|}{\| x_{D_{ik}^{(\ell-1)}} - x_{D_{ik}^{(\ell-2)}} \|}, \quad \ell = 3,4,\ldots \tag{6}$$

where $x_{D_{ik}^{(\ell)}}$ refers to the horizontal or vertical part of d.p. estimate at $\ell$-iteration as defined by equation (5). The norm $\|\|$ is defined to be:

$$\| x_{D_{ik}^{(\ell)}} - x_{D_{ik}^{(\ell-1)}} \| = \frac{\left| x_{D_{ik}^{(\ell)}} - x_{D_{ik}^{(\ell-1)}} \right|}{atol + rtol * \left| x_{D_{ik}^{(\ell-1)}} \right|}$$

The parameters $atol$, $rtol$ are two predefined numerical tolerances, absolute and relative respectively. They express the level of error we consider sufficient to accept that the algorithm has converged to the solution. With the norm above defined, we can implement a control strategy such as the one broadly described (in a simplified way) by Algorithm 1. A minimum of 2 iterations is done with a maximum up to *NDPI* where the latter can be for example 5 or 10. Separate convergence tests are applied in the horizontal and in the vertical, however, for simplicity this is not evident in Algorithm 1. Iterations stop updating the solution when both tests have been satisfied. More specifically, when the convergence rate of iterations begins to deteriorate, i.e. when it exceeds 0.5, either in the horizontal or vertical direction then updates of d.p. in this direction freeze but they continue in the other direction. Once decided that a gridpoint must terminate at the $k^{th}$ iteration (either due to convergence or divergence of the iterative procedure) then iterations continue to the maximum allowed number *NDPI* but $k+1,\ldots,NDPI$ will reproduce identical d.p. estimates with $k$. This appears wasteful but we must take into account that convergence may vary considerably from gridpoint to gridpoint and the extra "idle" iterations are simply used to prevent load balancing problems between computer nodes. So, practically we do not gain in efficiency but the expectation is that stopping "harmful" diverging iterations may be beneficial. Additionally it provides a tool to examine how many iterations are needed to achieve convergence within a pre-specified accuracy requirement.

To test this algorithm the forecast case of 5 July 2014 is used where the parameter NDPI is set to a large number 10 in order to examine how many DPI the model chooses to achieve convergence on specified accuracy criteria. Results from two runs are presented in Fig. 7a-d: one with pure absolute error control atol=1.0e-10 (rtol=0) and one with mixed absolute/relative error control atol=1.0e-10 and rtol=1.0e-6. The number of DPI computed dynamically by this method at each gridpoint of model level 115 (approximately at 850 hPa height) at t+96 hrs is plotted for both the horizontal and vertical dimension. The plots demonstrate the expected sensitivity to user tolerances i.e. for the strict tolerance run atol=1.0e-10 larger number of iterations is selected. Nevertheless, despite this tolerance dependency, a similar pattern is obtained in both cases. The largest number of iterations occurs above the Andes, the

Himalaya, the Rockies, the Antarctic coastline and above the southern ocean storm track. The number of DPI approach the maximum allowed number for this experiment around the core of typhoon Neoguri. This is illustrated in Fig. 7e-f. Comparing the previous figures with Fig. 4 we observe a contradiction: the latter shows that as iterations progress the scaled difference $\delta x^{(\ell)}_{D,ik}$ appears to reduce in size more slowly in the vertical rather than the horizontal suggesting that it is more difficult to converge in the vertical. However, when dynamic DPI is used, slightly more iterations are needed in the horizontal. This is explained by the fact that for some gridpoints the estimated vertical convergence rate ($cr$) may exceed at an iteration the 0.5 threshold and therefore iterations stop there never reaching the maximum allowed number (diverged iterations, see Fig. 7g-h). On the contary, in the horizontal, despite that the convergence is slow, there are very few diverged iterations and therefore the maximum number can be reached.

Forecast verification experiments with this scheme gave mostly neutral results in terms of forecast skill. However, this strategy seems to have big impact in the so called tangent-linear model used in the 4DVAR system when the number of DPI increases as will be explained in the next section.

**Algorithm 1** Convergence test for d.p. iterations

**while** $\ell \leq NDPI$ **and** $\ell > 2$ **do**
  **if** $\ell > 2$ **and not** (*diverged* **or** *converged*) **then**
    *compute cr*;
    **if** $cr > 0.5$ **then**
      *current d.p. has diverged;*
      *stop updating current d.p.;*
    **else**
      *update d.p.*
      **if** $\|x^{(\ell)}_D - x^{(\ell-1)}_D\| < 1$ **then**
        *d.p. converged;*
        *stop updating current d.p.;*
      **end if**
    **end if**
  **end if**
**end while**

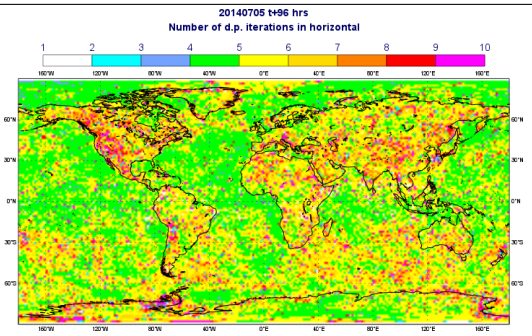


(a) horizontal atol=1e-10

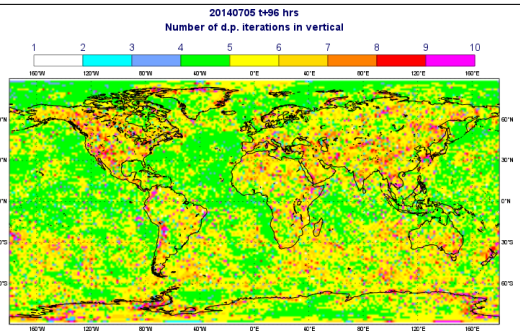


(b) vertical atol=1e-10

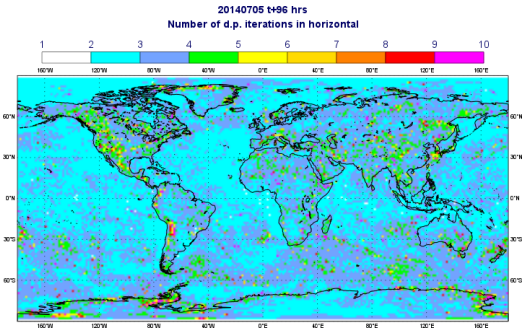


(c) horizontal atol=1e-10,rtol=1e-6

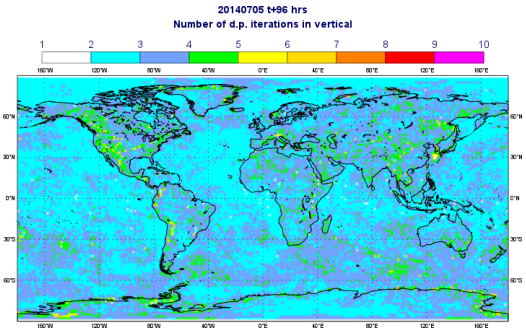


(d) vertical atol=1e-10,rtol=1e-6

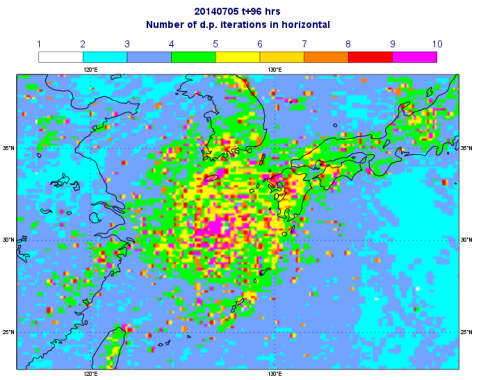


(e) horizontal atol=1e-10,rtol=1e-6

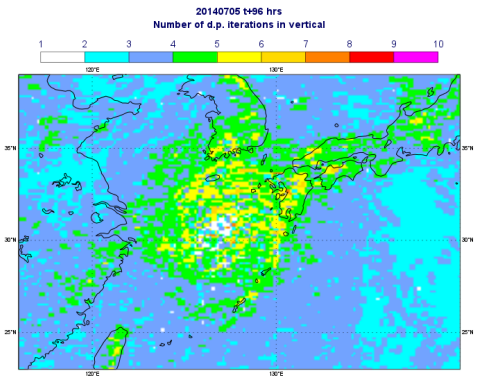


(f) vertical atol=1e-10,rtol=1e-6

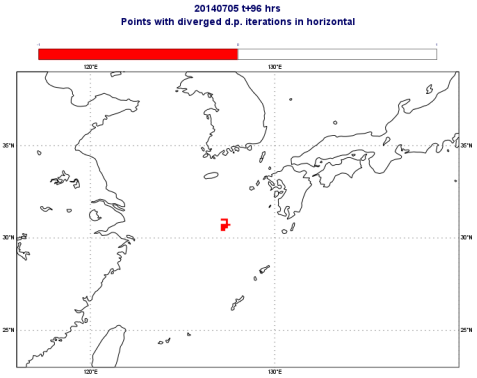


(g) Gridpoints with diverged horizontal DPI

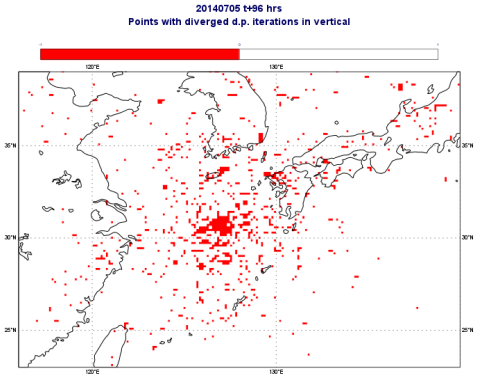


(h) Gridpoints with diverged vertical DPI

Figure 7: Dynamically computed number of DPI at t+96 hrs step in the horizontal/vertical at 850 hPa height (model level 115). Plots (a)-(d): global region. Plots (e),(f): vicinity of Typhoon Neoguri. White colours correspond to 2 iterations while purple to 10. Plots (g),(h): gridpoints (coloured red) where iterations diverged.

# 5 Departure point iterations and impact on the tangent linear model

IFS is using a 4-dimensional variational data assimilation (4DVAR) system to compute the initial state of the atmosphere (see Rabier et al., 2000). A central component of this system is the "Tangent Linear" model (TLM) and its adjoint. These two models are used in a minimization procedure to compute the atmospheric state that provides the best fit of a short range background forecast to available observations within a 12-hour assimilation window. The TLM is derived from the nonlinear forecast model (NLM) linearized around the best available estimate of the atmospheric state (the "trajectory") and is used to evolve analysis increments over the assimilation window. The TLM employs a linearized set of physical parametrizations (Janiskova and Lopez, 2012). The TLM code for the SL dynamics is derived directly from the NLM code using a line-by-line approach i.e. every line of the discrete NLM code is converted to the discrete TLM code and from this we derive the adjoint code.

Tests of the 4DVAR system with a large number of iterations, i.e. in both the NLM and the TLM/adjoint model, revealed occasional instabilities in the TLM that may result in forecast failures. Separate stand-alone tests of the TLM confirmed these instabilities, showing that, in some cases of strong stratospheric cross-polar flow, fast amplifying noise emerges spreading in three dimensions "contaminating" the solution in a large region of the atmosphere.

There is a link between the occurrences of this flow-generated noise and non-converging DPI. Experimentation suggests that doing a large number of iterations with the TLM on a gridpoint where the corresponding NLM trajectory (linearization state) had difficulties converging is what excites this instability. Therefore, a logical step forward would be to apply consistently the convergence control and dynamic DPI approach described in the previous section to the 4DVAR system as well. Indeed, this technique seems to effectively control this instability and the system can be run stably with an increased number of iterations. The implementation for the TLM scheme can be summarized in two steps and resembles a master-slave process:

1. the NLM computes the linearization state (trajectory) and during this computational process determines dynamically the number of required DPI per gridpoint and saves this number;
2. the previously computed number of DPI is used for the TL and adjoint models at corresponding gridpoints. For example, if up to 10 iterations are allowed but the NLM at gridpoint *ik* "decides" 3 iterations are required for the trajectory then the TLM/adjoint at this gridpoint will be restricted to do 3 iterations.

The TLM instability and the impact of DPI control is demonstrated in Fig. 8 where as suggested by Li et al. (1993) the difference

$$D[\delta x(t_0)] = M'(t_n,t_0)\delta x(t_0) - \{M(t_n,t_0)[x_0(t_0)+\delta x(t_0)] - M(t_n,t_0)[x_0(t_0)]\} \tag{7}$$

is plotted at t+12hrs for temperature ($x = T$). The first term in the right-hand-side of Eq. (7) denotes the TLM ($M'$) evolution of a perturbation $\delta x(t_0)$ from a basic state $x_0(t_0)$ in the time interval $[t_0,t_n]$ and the remaining term the difference between the perturbed and unperturbed NLM ($M$) forecast. From the definition of the TLM, we expect that ideally for a small perturbation the difference $D[\delta x(t_0)] \to 0$ for any prognostic variable $X$. Of course, in practice this does not happen given that NWP models have limiters in dynamics and branch functions in parametrizations (discontinuous derivatives). Nevertheless, we expect that $D$ should be bounded and small. When the norm of this difference increases, then the TLM becomes a poor approximation to the NLM and the quality of the analysis deteriorates. The resolution of our test case is TL255 ( 80km which matches the resolution of the TLM at operational IFS model cycle

41r1) and the initial time of the forecast is 00 UTC at 2 October 2013. When the number of DPI (NDPI) increases from 2 to 5 and then to 10 we see that $D$ grows excessively near the southern pole unless we apply dynamic DPI control. This instability, which occurs only in the TLM, is also evident at the t+12 hrs wind field at vertical level 20 (3 hPa) plotted in Fig. 9. We notice that although for the NLM there is very little difference in the runs with NDPI=2 and 10 (plots (a) and (b)), there is a huge difference for the corresponding evolved TLM increments (plots (c) and (d)) which are clearly the result of an unstable computation when NDPI=10. Halving the timestep removes the instability but of course at the cost of doubling the CPU time. Iteration control is equally effective having a negligible impact in CPU cost. For this test we have used a near zero absolute tolerance ATOL=1.0E-15 (approximately double precision machine accuracy) and RTOL=0. This setting essentially forces the algorithm to keep iterating up to NDPI unless it detects an insufficient convergence rate or the difference between two successive estimates for the d.p. is smaller than machine double precision. Analysis of the results for this case show that diverging iterations are concentrated near the pole at the upper levels of the stratosphere where the instability in the TLM occurs. These are detected early by the algorithm and the number of iterations are restricted usually to 2 on these gridpoints. Computing the horizontal Lipschitz number:

$$\Delta t \max(u_x, u_y, v_x, v_y)$$

at vertical model level 20 in the stratosphere (3 hPa) we found that for a few points near the pole it slightly exceeds 1 (plot not included). This happens for the number associated with the $u_x$ and $v_x$ components. Note that such issues with the TLM instabilities are not entirely unexpected. For example, Li et al. (1993) quote that "the TLM is more likely to break down in regions where sharp gradients prevail in the interpolated fields coupled with strong advective wind".

To demonstrate the impact of increased number of iterations in the 4DVAR components, results from 2-months boreal winter experiments at TL1279 resolution are shown in Fig. 10. The control experiment uses 5 dynamic DPI in all model components and the other one uses 5 iterations only in the NLM (fixed at all gridpoints). The figure shows the normalised difference for the RMSE of the geopotential at 500 hPa, validated against the analysis produced by each experiment (negative values indicate a reduction of the RMSE with respect to the first experiment). The results shows a (small) further reduction in the forecast error when 5 iterations are used across all model components. However, the spatial structure of this reduction is not confined to the area where the reduction of the error occurs when the number of DPI is increased from 2 to 5 and it is not entirely understood. The mechanism behind the improvement needs to be further investigated. It could be either related with improved consistency between the TLM and NLM i.e. by using exactly the same setting the TLM approximates more accurately the NLM which in turn improves analysis and forecast, or it could be the result of running with dynamic DPI during this period.

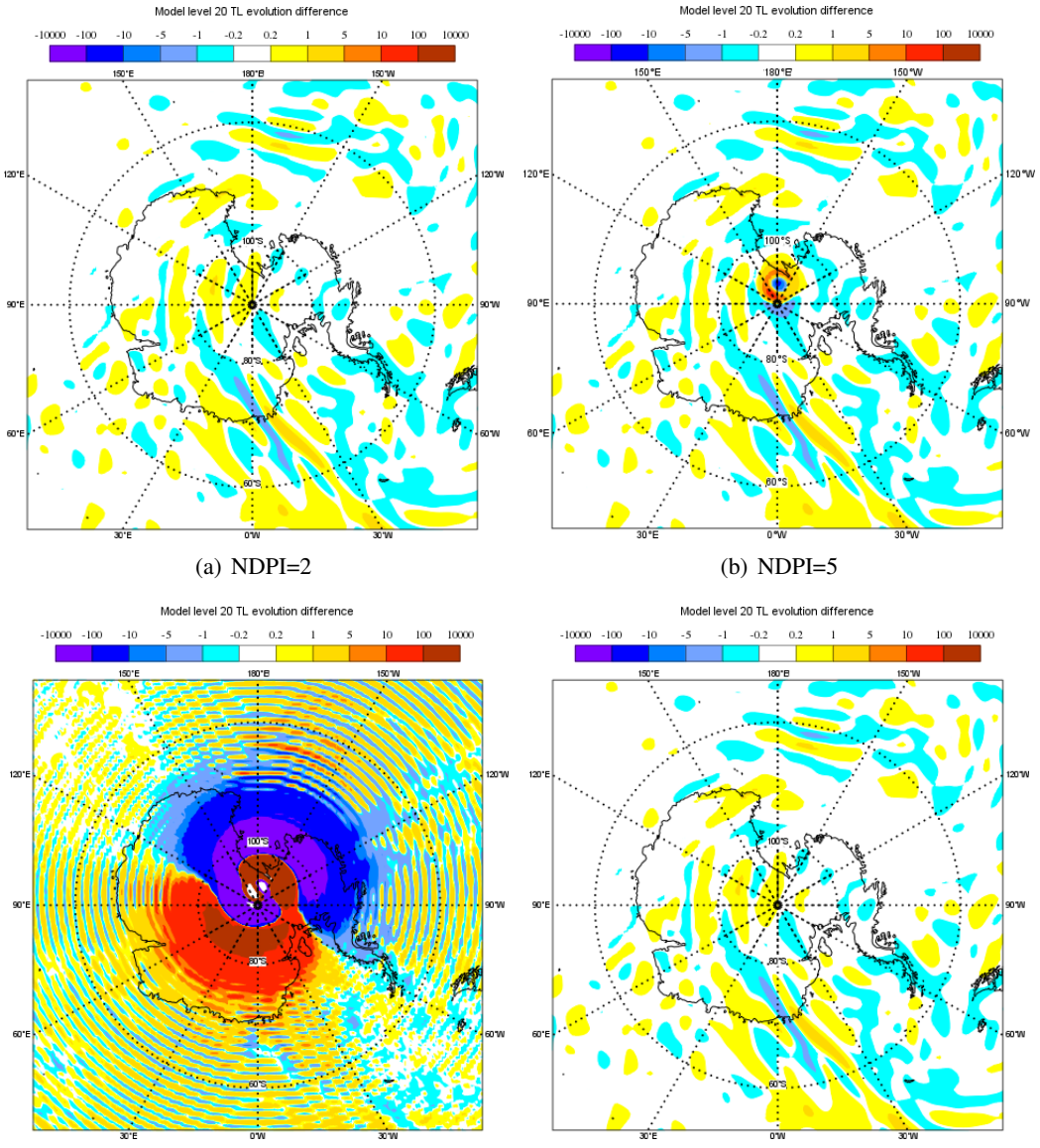


(a) NDPI=2 (b) NDPI=5

(c) NDPI=10 (d) NDPI=10 with dynamic selection

Figure 8: Tangent linear - non linear model perturbation difference for temperature, $D[\delta T(t_0)]$, at time t+12 hrs and model level 20 (3 hPa); (a)-(c) using different numbers of d.p. iterations (NDPI); and (d) including the convergence control algorithm.

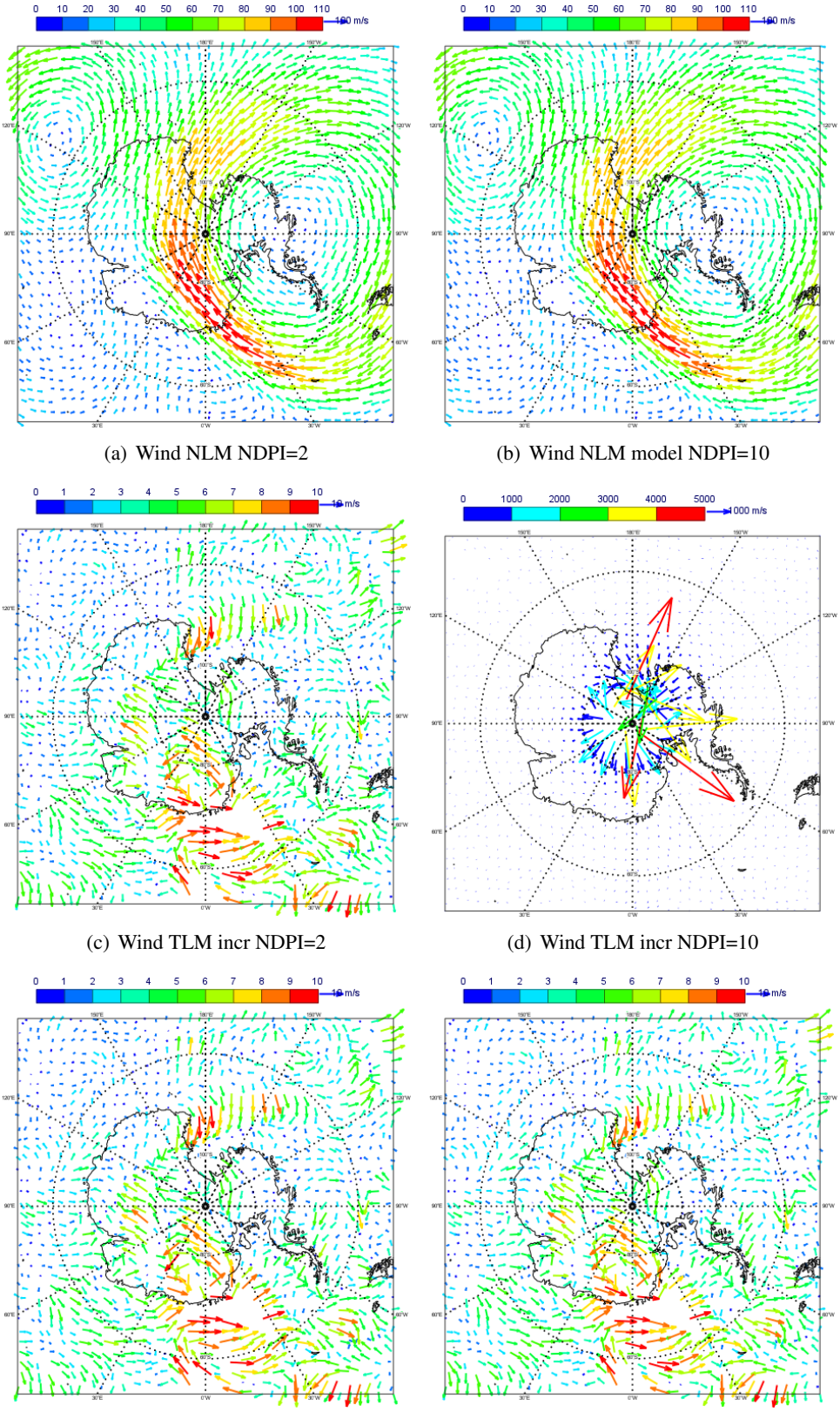


(a) Wind NLM NDPI=2

(b) Wind NLM model NDPI=10

(c) Wind TLM incr NDPI=2

(d) Wind TLM incr NDPI=10

(e) Wind TLM incr NDPI=10, $\Delta t/2$

(f) Wind TLM incr NDPI=10 dynamic selection

Figure 9: Plots (a), (b): model level 20 (3hPa) wind vectors coloured by wind speed at t+12 hrs from a non-linear model (trajectory) forecast with 2, 10 number of d.p. iterations (NDPI); and (c)-(f): tangent-linear model perturbation around the trajectory wind field evolved in a 12 hrs window with NDPI=2,10,10 with 1/2 the timestep, 10 with dynamic DPI respectively.

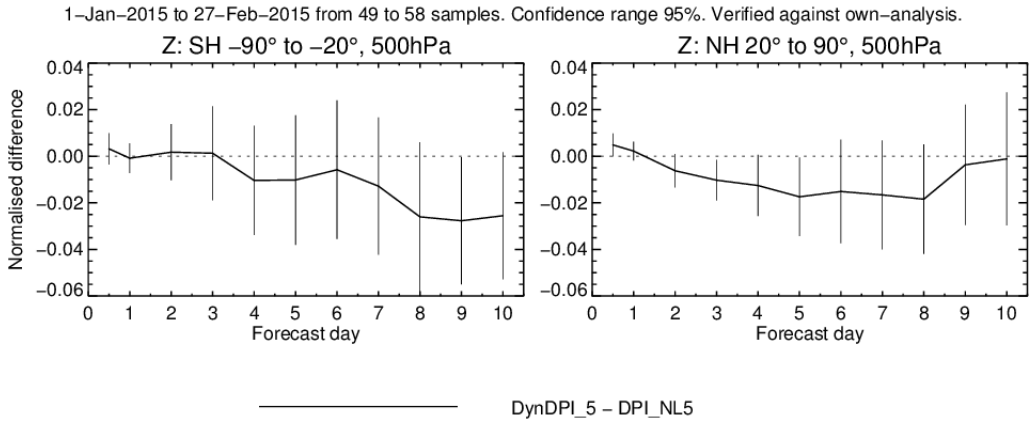


(a) NH/SH z 500hPa RMSE

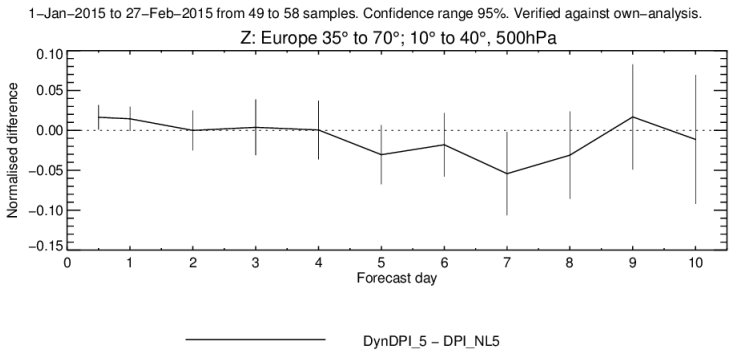


(b) Europe z 500hPa RMSE

Figure 10: Normalised difference of RMSE for 500hPa geopotential height of experiment “DynDPI_5” (5 dynamically selected d.p. iterations in all model components) from experiment “DPI_NL5” (5 fixed d.p. iterations for all gridpoints in forecast model and 2 in 4DVAR tangent-linear and adjoint model components). (a) For NH/SH. (b) For Europe. Negative values indicate that the first experiment has reduced RMSE compared with the second.

# 6 Conclusions

In this report we challenge the typical assumption that 2-3 iterations of the scheme used to compute the departure points in a high resolution semi-Lagrangian model with large timesteps are sufficient. We demonstrate statistically significant forecast improvements by increasing the number of iterations, mostly in the troposphere over regions where a strong jet stream crosses mountain ranges. By increasing the number of iterations to 5 we found reduced forecast errors connected to such features.

Large sensitivities to the number of iterations were also found around tropical cyclones, which is not surprising as both horizontal and vertical velocities are extreme. The error introduced by the advection scheme seems to give rise to instabilities in the vertical structure of the atmosphere. These lead to extreme vertical transport reaching far up into the stratosphere and give large errors in the humidity e.g. on 50 hPa level. By increasing the number of iterations these instabilities were supressed yielding a clear improvement in the stratosphere above regions with tropical cyclone activity.

For consistency in the forecasting system, it is desirable to use the same number of d.p. iterations in data-assimilation as in the forecast. However, the tangent-linear model of the ECMWF 4DVAR data assimilation system was found to be more sensitive in situations where departure point iterations did not converge (or rather diverged). A natural step was to investigate whether using a "dynamic" in space and time selection of the number of iterations could be beneficial. It was found that while the impact of this in the non-linear model is marginal there was a big stabilising effect in the tangent-linear model for runs where iterations are increased. However, from the operational point of view, dynamic selection of departure point iterations remains at this stage a research tool mainly due to the fact that most benefit in forecast accuracy has been realised by increasing the number of departure point iterations in the non-linear model. The forecast improvements demonstrated here are also broadly manifested at lower resolutions provided that the ratio of timestep to resolution is relatively large (implying large mean Courant numbers and relatively large Lipschitz numbers).

To conclude, this report has demonstrated the benefit of increasing the number of departure point iterations in the semi-Lagrangian scheme. As a result of this, a change was introduced in IFS model cycle 41r2 to increase the number of departure point iterations in the non-linear model from 3 to 5. The resulted improvement in the accuracy and better convergence of the departure point iterations allowed a slight increase of the model timestep from 400s to 450s in the 9km horizontal resolution model (to be operational in 2016) without noticeable impact in forecast accuracy and hence reduce the computational cost of the forecast. Although the results presented here are specific to the ECMWF model IFS, we believe that our findings apply to other weather prediction models using semi-Lagrangian techniques.

# Acknowledgements

Useful advise given by Drs E. Holm, P. Lopez and F. Vana at ECMWF for the implementation and testing of the tangent-linear and adjoint part in this work is gratefully acknowledged as well as feedback by Dr. Sylvie Malardel on the impact of this work in high resolution forecasts. We would also like to thank Drs S.J. Lock and N. Wedi at ECMWF for providing comments on the manuscript.

## References

Diamantakis, M. (2014). Improving ECMWF forecasts of sudden stratospheric warmings. *ECMWF Newsletter No. 141-Autumn 2014*, 30–36.

ECMWF, R.-D. (2015). IFS documentation. https://software.ecmwf.int/wiki/display/IFS/CY41R1+Official+IFS+Documentation.

Hortal, M. (2002). The development and testing of a new two-time-level semi-Lagrangian scheme (SETTLS) in the ECMWF forecast model. *Q.J.R. Meteorol. Soc. 128*, 1671–1687.

Janiskova, M. and P. Lopez (2012). Linearized physics for data assimilation at ecmwf. *Data Assimilations for Atmos., Oceanic and Hydrologic Applications 2*, 251–286.

Li, Y., I. M. Navon, P. Courtier, and P. Gauthier (1993). Variational data assimilation with a Semi-Lagrangian Semi-Implicit global shallow-water equation model and its adjoint. *Mon. Weather Rev. 121*, 1759–1769.

Pudykiewicz, J. A. and A. Staniforth (1984). Some properties and comparative performance of the semi-Lagrangian method of Robert in the solution of the advection-diffusion equation. *Atmos. Ocean 22*, 283–308.

Rabier, F., H. Järvinen, E. Klinker, J. Mahfouf, and A. Simmons (2000). The ECMWF operational implementation of four-dimensional variational assimilation. part i: experimental results with simplified physics. *Q.J.R. Meteorol. Soc. 126*, 1143–1170.

Smolarkiewicz, P. K. and J. A. Pudykiewicz (1992). A class of semi-Lagrangian approximations for fluids. *J. Atmos. Sci. 49*, 2082–2096.

Staniforth, A. and J. Côté (1991). Semi-Lagrangian integration schemes for atmospheric models - a review. *Mon. Weather Rev. 119*, 2206–2223.

Temperton, C., M. Hortal, and A. Simmons (2001). A two-time-level semi-Lagrangian global spectral model. *Q.J.R. Meteorol. Soc. 127*, 111–127.

Wedi, N., P. Bauer, W. Deconinck, M. Diamantakis, M. Hamrud, C. Kühnlein, S. Malardel, K. Mogensen, G. Mozdzynski, and P. Smolarkiewicz (2015). The modelling infrastructure of the Integrated Forecasting System: Recent advances and future challenges. Technical Report 760, ECMWF.